# Contact Plan Design for GNSS Constellations: A Case Study With Optical Intersatellite Links

**ANDREA NARDIN**, Graduate Student Member, IEEE
Politecnico di Torino, Turin, Italy

**JUAN A. FRAIRE**, Senior Member, IEEE

**FABIO DOVIS**, Member, IEEE
Politecnico di Torino, Turin, Italy

**Optical Intersatellite Links (OISLs) are being considered for future Global Navigation Satellite System (GNSS) constellations. Thanks to OISLs, the constellation incorporates improved clock synchronization and precise ranging among the satellites, which are essential features to achieve accurate time and orbit determination. High data rate communications within the space segment also reduce ground segment dependency, by means of decentralized access to information. However, the dual optimization of data and navigation performance metrics requires a careful assignment of OISLs to the available laser communication terminals on-board. To this end, we present a contact plan design scheme based on a degree constrained minimum spanning tree heuristic applied to such OISL-enabled GNSS (O-GNSS) constellations. Results on the Kepler system, a novel GNSS proposal, show that a fair distribution of connectivity among the constellation can be ensured while optimizing its range-based position estimation capabilities (PDOP). A PDOP improvement of 85 % is reached on average by the optimized contact plan with respect to a generic scheduler that disregards the geometrical distribution of the chosen links.**

Manuscript received February 10, 2021; revised June 16, 2021 and September 3, 2021; released for publication November 1, 2021. Date of publication December 14, 2021; date of current version June 9, 2022.

DOI. No. 10.1109/TAES.2021.3135025

Refereeing of this contribution was handled by O. Osechas.

Authors' addresses: Andrea Nardin and Fabio Dovis are with the Department of Electronics and Telecommunications, Politecnico di Torino, 10124 Turin, Italy, E-mail: (andrea.nardin@polito.it; fabio.dovis@polito.it); Juan A. Fraire is with the Inria, INSA Lyon, CITI, Univ Lyon, F-69621 Villeurbanne, France, with the CONICET - Universidad Nacional de Córdoba, Córdoba C1425FQB, Argentina and also with the Saarland Informatics Campus, Saarland University, 66123 Saarbrückenn, Germany, E-mail: (juanfraire@gmail.com). *(Corresponding author: Andrea Nardin).*

This article has supplementary downloadable material available at https://doi.org/10.1109/TAES.2021.3135025, provided by the authors.



## I. INTRODUCTION

Global Navigation Satellite Systems (GNSSs) rely on satellite's clock synchronization to allow the successful positioning of users on ground [1]. Current GNSS satellites are equipped with atomic clocks that are continuously supported by a ground network of monitoring stations in charge of estimating their offsets. Computed corrections are provisioned to the satellite and inserted in the navigation message [2]. Because of ground station costs and the impairments provoked by the atmosphere on the received signal (multipath and delay), the concept of an independent flight segment has attracted the attention of the research community [3]–[7].

A promising solution to autonomously synchronize and connect future GNSS satellites are Optical Intersatellite Links (OISLs). Thanks to two-way time and frequency transfer techniques at high rate [8], 1) accurate clock distribution among connected laser terminals can be accomplished with unprecedented levels [9]. Furthermore, laser transceivers facilitate sub-mm ranging, which enables 2) enhanced orbit determination [10]. The improved synchronization and orbit determination capabilities of the space segment shall enable a superior positioning and timing performance attainable by the users with respect to current GNSSs [8]. On the other hand, as we argue later in this article, the high data-rate optical communication channel can be also used to network the medium-earth orbit (MEO) GNSS satellites with an always reachable supporting fleet, which could be placed at a different orbital altitude, on a low-earth orbit (LEO), high-earth orbit (HEO), or geosynchronous orbit (GSO). Besides serving as 3) in-orbit integrity monitoring stations for the navigation signal, supporting satellites can act as a 4) connectivity backbone for the constellation, which minimizes the dependency on the ground segment (as a reference, GPS requires 11 command and control plus 16 monitoring stations [11]). The combined benefits in 1)–4) are already attracting the attention of the designers of future GNSS constellations [12]. Indeed, the recent GNSS project named Kepler [5] is the first to embrace these principles, which motivates future GNSS satellite constellations to follow:

One of the main challenges of an OISL-enabled GNSS (O-GNSS) is that the satellites are equipped with a limited set of highly directional laser communication transceivers (LCTs). LCTs are typically mounted on mechanical gimbal platforms to point the optical aperture and track the target satellite, which must likewise be prepared and pointed in order to successfully establish and maintain the optical channel contact. As a result, OISLs require larger gimbal swipes than radio-frequency (RF) systems, more precise positioning in the target angle, and more complex acquisition mechanics typically based on divergent beaconing and spiraling [13] that require special consideration of the link establishment period in the planning phase. Unfortunately, combined orbital mechanics, gravitational perturbations, station-keeping maneuvers, mission parameter changes, and the dynamic relative orientation of the satellites forbid

the consideration of fixed-configuration mechanisms based on periodicity. Instead, a persistent planning process is required so that the utilization and pointing information of available LCTs is continuously decided and timely provisioned to the satellite constellation in advance. The contact planning must consider the overall system-level implications of the chosen links, as they affect the aforementioned navigation precision and data connectivity metrics. Thus, the efficient contact plan design (CPD) [14] is crucial to ensure the benefits that gave rise to future GNSS constellations enhanced by OISLs.

The main contribution of this article is to unlock the CPD bottleneck. In particular, this article introduces an overcoming and generic method for CPD optimization addressed to future O-GNSS constellations, taking also into account LCTs limitations and constraints. The proposed method applies to those constellations whose MEO satellites present a number of continuously established links (e.g. neighboring satellites on the same orbital plane) and a single link subject to scheduling, which might be dedicated to a backbone access or to a MEO interorbital connection. Our algorithm is based on a solution of the degree constrained minimum spanning tree (DCMST) problem [15], [16], to deliver a connected GNSS constellation topology where a positioning quality factor is exploited as a driving metric. Through the investigation of four different scenarios, with variable LCT limitations and size of the supporting fleet, we can explore the flexibility of our approach also within a specific case study. Results on the Kepler case show that the approach delivers an improved OISL utilization schedule and is easily tractable in terms of computation effort.

The rest of the article is organized as follows. Section II provides the background on GNSS supported by OISLs, as well as the state-of-the-art of CPD techniques. Section III focuses on the criteria used in the CPD to meet system requirements and constraints. The topology model is then defined to be used in Section IV, where the CPD method is presented. The results from the CPD algorithms applied to realistic GNSS scenarios are reported in Section V and finally, Section VI concludes this article.

## II. BACKGROUND

The space segment of traditional GNSSs comprises a set of several MEO satellites. In some cases, Geostationary Orbit (GEO) and Inclined GSO satellites are also part of the space segment [17], [18]. The ground segment, on the other hand, includes several ground stations for monitoring the constellation and commanding with each individual satellite. However, intersatellite links (ISLs) are already featured in modern GNSSs to foster the space segment autonomy [6], [7], [18], [19]. Present and next GNSS generations are giving an increasingly important role to ISLs. Indeed, as discussed in [4], RF-based ISLs are already equipped in third-generation GPS [20] and BeiDou satellites [18], are being considered in European GNSS [21], [22], and have received significant attention from the research community [23]–[25].

One of the main reasons for using ISLs lies in the fact that GNSS autonomy can be largely increased if the dependency on the ground segment is reduced. In particular, this can be achieved if ranging (to enhance autonomous navigation and orbit determination) and data transfer (to enable in-orbit clock synchronization and to relay telemetry and commands to and from satellites out of range from the ground station) can be efficiently delivered via multihop ISLs.

### A. GNSS Supported by OISLs

OISLs are emerging as the evolution of RF ISLs and they are already a reality for the Chinese GNSS [19]. By operating at smaller wavelengths (1550 nm and below), a more directional beam can be achieved with a smaller aperture. The results are higher data rates (in the order of Gbps) and enough spatial diversity to avoid an already congested RF spectrum. Optical links are already operational or under validation for satellite-to ground downlinks [26]–[28], satellite-to-satellite-links [29], and even deep space links [30]. Most recently, the miniaturization of optical communication payloads is showing promising advances towards its consideration for data transfer from nano satellites [31].

Indeed, laser-based time transfer experiments show that 0.1 ps accuracy level can already be achieved [32]. Thus, GNSS satellites can share fine satellite clock information modulating the optical signal accompanied with ephemeris data. The continuous flow of information reduces the accuracy (and costs) required for on-board clocks, which no longer need to be atomic. As a result, O-GNSS constellations are expected to further reduce the ground infrastructure dependency.

The idea of including a LEO backhaul as a support for the GNSS network has been introduced in the context of the Kepler constellation. The approach has recently attracted the interest of the research community [5], [8], [10], [12], and will inspire future GNSS features. The LEO backbone space segment carries long-term stable optical clocks and is accessed through bidirectional OISLs from the MEO segment. As a result, the LEO backbone enables a direct clock synchronization among satellites as well as a precise optical ranging improving orbit determination. Furthermore, the LEO segment can also be exploited for integrity monitoring of the navigation signal before it is affected by the atmosphere, among other purposes further discussed in [12]. The space segment of the Kepler system is illustrated in Fig. 1, in its version with four LEO satellites, according to the parameters reported in [12].

In particular, the Kepler system is designed with 24 MEO satellites distributed over three orbital planes. This GNSS also includes a set of four-to-six LEO satellites, whose orbital parameters are also reported in [12]. Each MEO satellite in Kepler is equipped with three LCTs. Two of them are directed towards each of the two neighbors on the same orbital plane, one ahead and one behind the flight direction. This ensures the continuous connectivity of each

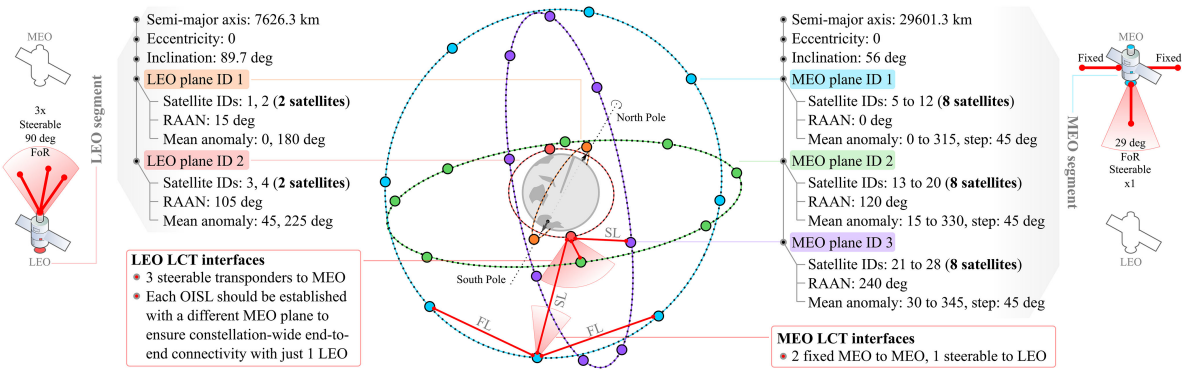


Fig. 1. Kepler GNSS constellation supported by OISL and a LEO backbone segment composed by 4 satellites.

set of 8 MEO satellites in the same plane. The third LCT is pointed toward nadir (earth) direction to establish a two-way link with one of the LEO satellites. On the other hand, each LEO satellite in the fleet is provisioned with a set of three steerable LCTs pointed to the zenith vector of the spacecraft. Thus, each MEO in Kepler can link to a single LEO, but each LEO is able to connect simultaneously at most three MEO satellites from three different orbital planes. Thanks to this topology, persistent multihop connectivity of all MEO GNSS satellites is possible in Kepler. Nonetheless, a similar result can be obtained without a backbone fleet, using instead interorbital connections that link MEO satellites on different orbital planes.

### B. Contact Plan Design

To profit from the aforementioned navigation and data transfer benefits, a careful assignation of LCT pairs among satellites is required for GNSS constellations supported by OISLs [12]. The general link selection under constrained resources in intermittent and partitioned networks is a well-known problem called CPD. The objective of the CPD is to select the pair of nodes between which a contact shall be established by means of limited resources (e.g., amount of available transponders or antennas) to meet an overall system-level goal. The topic has enjoyed an increasing interest of the academic community, including a series of publications focused on modern GNSS constellations supported by ISLs. CPD was first applied to GNSS in 2011 considering both ranging and communication needs to support autonomous navigation [33]. The minimum of position dilution of precision (PDOP), a geometrically determined factor affecting the positioning error, was then introduced in the CPD process in [34]. Heuristics were developed to include navigation precision but also information transmission delay and integrity into genetic algorithms to decide upon ground-to-space GNSS links [35]. Simulated annealing was also applied in [36] to tackle position requirements combined with multihop data delivery efficiency, when routed based on contact graph routing techniques. In all the cited works, time is slotted, thus, contact assignations are delivered in a discrete set. To enhance the flexibility of the approach, recent research proposed cascade methods to iterate over and optimize slot lengths [37]. This last paper proves the efficiency of the network can be increased two-fold with respect to the fixed time slot in [36]. Other derived algorithms in the literature include deterministic constructive [38], double-loop [39], grouping methods [40], and multistage algorithms [41].

The main limitation of the aforementioned efforts is that they were focused on a single hierarchy of MEO satellites equipped with RF transponders with wide signal coverage (i.e., no fine-pointing or beaconing/spiraling needed). In this article, we extend the CPD to GNSSs where connectivity is realized by highly directional point-to-point OISLs, taking into account as design parameters also the time constraints related to the pointing phase. To the best of authors' knowledge, none of the existing CPD techniques considered the constraints of GNSSs with OISLs through a networkwise optimization where an improved position determination is set as the primary objective of the CPD. Only Giorgi *et al.* [12] addressed the issue for the Kepler constellation with greedy approaches. This motivated us to use this LEO-supported O-GNSS as a natural case study for our work, taking advantage of existing scheduling algorithms as a term of comparison.

Although Kepler is a concrete and relevant case study, the same principle of supporting fleet in LEO can be generalized to other orbits and topologies, such as HEO or GSO. To this end, we generalize the Kepler scenario to any GNSS constellation with the OISL feature, where MEO satellites present, alongside continuously enabled links, a single freely-schedulable link, whether the latter is providing a backbone access (as in Kepler) or an interorbital link toward another MEO satellite.

## III. SYSTEM MODEL

An O-GNSS network renders several communication windows (a.k.a. contacts) among the satellites. We can distinguish such connections in the following:

1) *Fixed Links* (FLs), that are continuously established.
2) *Schedulable Links* (SLs), whose availability is time-dependent and thus primarily interested by CPD.

Links between neighboring satellites lying on the same orbital plane belong to the first category. It should be noted that typical GNSS satellites operate under the so-called yaw-steering (YS) attitude mode. In the YS mode, the spacecraft performs a continuous rotation about the earth-pointing ("yaw") axis such as to keep the solar panel axis perpendicular to the Sun direction [42]. Under such a configuration, along-track fixed links would need to be mounted on a gimballed (hemispherical) configuration that counter-rotates with respect to the rotation needed to align the solar panel.

On the other hand, interorbital MEO links or backbone-to-MEO links belong to the second one. Fig. 1 provides an example of such classification applied to the Kepler system. In case of a backbone-supported GNSS network, the SLs would be both dynamic and sporadic since the orbital periods of backbone satellites can be shorter or longer than those at MEO.

As satellites' positions evolve over their orbital trajectory, it is necessary to select which SLs shall be established to connect the entire constellation. Based on accurate orbital propagators, the contact plan can be derived in advance, computed on ground, and timely provisioned to the constellation. This process needs to be repeated when new relative geometries among satellites arise due to perturbations and unmodeled phenomena. To exploit the potential of such a system, a well-designed contact plan for SLs is of utmost importance. It can favor profitable ranging conditions and should guarantee the connectivity of the whole network, which in turn ensures continuous system-wide clock synchronization. Thus, a successful CPD is a key feature to reduce ground segment dependency [4].

### A. Optimization Metric

The CPD can exploit the degree of freedom that comes from the simultaneous availability of several potential SLs to optimize specific metrics of the GNSS constellation. In particular, intersatellite range observations have been already exploited to enhance the orbit determination process of GNSS satellites [6], [43]–[46]. In this case, orbit determination is generally performed by integrating ISL ranges and L-band ground measurements, which are often essential because at least one space-ground link or L-band observation from ground is necessary to avoid translational and rotational invariance of the whole constellation [43], [46]. Overall, the specific relationship between range observations and orbit estimation quality depends on the combination method employed. However, as also remarked in [47], a general metric to measure the impact of intersatellite ranging performance has not been deeply investigated.

To describe the dependency of the estimated position on range observations geometry, a well-known figure of merit in the GNSS literature is the Dilution of precision (DOP) [1]. Several formulations of DOP exist [48] and their use depends on the quantity of interest. For a synchronized system, as any GNSS space segment is [1], one of the the most meaningful figures of merit is the PDOP, a quantity that describes the dilution factor over the $x$, $y$, and $z$ axes. The PDOP is derived at each discrete time instant $n$ from the jacobian matrix $\mathbf{H}_{i,n}$. This matrix relates $N$ ranging measurements, computed from the target satellite $i$, to its three-dimensional position information [1]. It is defined as

$$\mathbf{H}_{i,n} = \begin{pmatrix} h_{x_1} & h_{y_1} & h_{z_1} \\ h_{x_2} & h_{y_2} & h_{z_2} \\ \vdots & \vdots & \vdots \\ h_{x_j} & h_{y_j} & h_{z_j} \\ \vdots & \vdots & \vdots \\ h_{x_N} & h_{y_N} & h_{z_N} \end{pmatrix} \tag{1}$$

where the elements in $(h_{x_j} h_{y_j} h_{z_j})$ define the direction cosines of the vector that from the satellite $i$ points toward the $j$th neighboring satellite from which the range is measured. All the principal diagonal elements of $(\mathbf{H}_{i,n}^{\intercal}\mathbf{H}_{i,n})^{-1}$ relate the ranging error to the position error over $x, y, z$ coordinates. Therefore, when ranges are computed in a completely synchronized system, the metric is determined as follows:

$$\mathrm{PDOP}_{i,n} = \sqrt{tr((\mathbf{H}_{i,n}^{\intercal}\mathbf{H}_{i,n})^{-1})}. \tag{2}$$

The lower the value in (2), the smaller the error multiplication due to geometrical dilution. On this basis, the minimization of the PDOP as a CPD figure of merit has been already investigated in the satellite navigation domain [4], [19], [34], [41], [47]. In this article, the use of PDOP as the geometrical indicator of the ISL contribution to orbit determination enables an optimization process, which is in line with the recent literature and prescinds from the underlying orbit determination algorithm, fostering some flexibility in the choice of the latter.

### B. Constraints

A feasible contact plan must fulfill the constraints that characterize an O-GNSS. A list of the main constraints for the optical links has been drawn in [12] for the Kepler system. These constraints fit the general case and they are, therefore, reported below, after a mild generalization where needed.

- **C1**. The LCTs dedicated to SLs have a limited FoR. A maximum visibility cone with a given aperture $\alpha$ must be observed in the scheduler algorithm.
- **C2**. Time is required to point (i.e., spiraling/beaconing), establish, lock, and stabilize the optical channel. This defines the minimum link duration $t_{\min}$ required for each connection.
- **C3**. Each satellite can simultaneously link a limited number of satellites, according to the availability of its OISL transponders.

To provide a more insightful definition of the constraint **C2**, we define

$$t_{\min} = t_{\text{point}} + t_{\text{useful}} \tag{3}$$

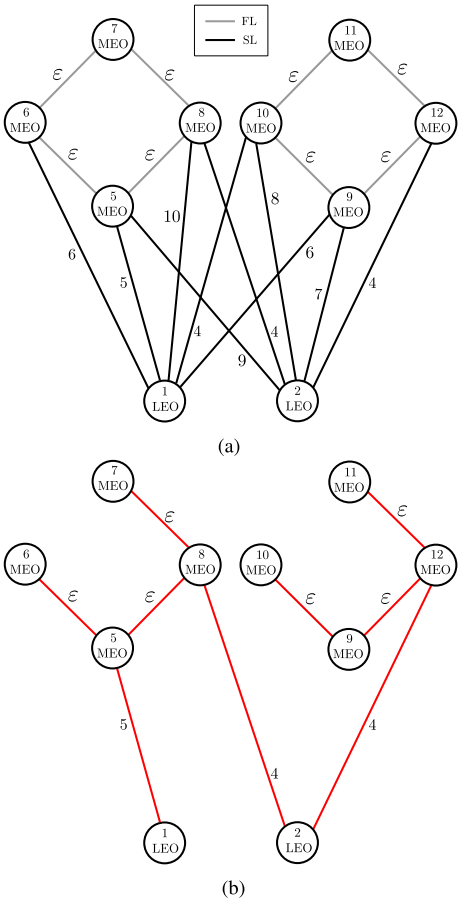


Fig. 2. Graph representation of a LEO-backhauled GNSS. (a) Graph. (b) Minimum Spanning Tree.

as the result of the time required to establish an optical connection $t_{\text{point}}$, added to the minimum amount of useful communication and ranging time that justifies the link pointing and establishment process. Specifically, $t_{\text{point}}$ is the delay imposed by the mechanical movement of the optical telescope gimbal from its current position to the direction of the target satellite, plus the link acquisition latency until bit-lock is achieved between the devices.

### C. Topology Model

An O-GNSS is generally a network of connected satellites whose OISLs are sporadic and irregular. Such a dynamic network can be modeled, according to graph theory [49], as a fully dynamic [50] graph $G_n = (V, E_n)$ where $V$ is the set of *nodes* (i.e., the satellites, comprising the main fleet in MEO as well as a possible supporting fleet) and $E_n$ is the set of *edges* (i.e., the optical links). In particular, the set $E_n$ is dependent on the discrete time $n$. In our model, each undirected edge represents a potential two-way link between two satellites at a given time instant. As a consequence, a graph $G_n$, like the one in Fig. 2(a), is a snapshot of the availability of the communication windows on the network at a certain time $n$.

If we are able to associate PDOP values to the weights of the edges, we can rely on graph theory and exploit properties and algorithms of weighted graphs to optimize the CPD w.r.t. PDOP. In fact, according to the requirements of the system under analysis, we would like to connect the whole network while minimizing the PDOP experienced by each MEO satellite. We need, therefore, to find a subset of $G_n$ that connects all nodes and minimizes the total weight of the edges, ensuring the overall best PDOP configuration attainable at the time $n$. This is precisely a minimum spanning tree (MST) [51] of $G_n$ [see Fig. 2(b)].

Setting the right weight to the edges is not trivial. The PDOP value is a function of $\mathbf{H}_{i,n}$ and, thus, it depends on the spatial distribution of all the satellites whose ranges are employed in the position computation. The resulting PDOP of satellite $i$ depends on all its active optical links at time $n$ and, thus, referring to the graph model, on its adjacent nodes. It is generally not possible to associate a single link (i.e., an edge) to a PDOP value since the latter is determined by more than one established connection. In the GNSS framework, however, we are interested mainly in the position estimation of MEO satellites, because their enhanced orbit determination will improve the navigation signals.

In Kepler for instance, MEO satellites are equipped with three LCTs, therefore, a $3 \times 3$ $\mathbf{H}_{i,n}$ matrix can be obtained for each $i$ belonging to the set of MEO satellites. Two rows of $\mathbf{H}_{i,n}$ correspond to the two FLs connecting a MEO satellite to its neighbors within the MEO plane (see Fig. 1). The third row models the idle LCT, which is dedicated to a possible backbone-to-MEO link (the SL). As a consequence, only the SL determines the resulting PDOP of a MEO satellite. This means that we can associate a single PDOP value to each edge of $G_n$, with the exception of edges that represent a FL. Indeed, FLs are not subject to scheduling and do not participate in the optimization process.

A single LCT dedicated to a backbone access or to a MEO interorbital connection is a reasonable assumption in O-GNSSs, given the mass and power characteristics of GNSS satellites. Moreover, the assignation of PDOP-dependent weights to edges suits also the case where SLs are not backbone-to-MEO connections (as in Kepler) but interorbital MEO links. In this case, a single interorbital link establishment would result in two distinct PDOP values for the two connecting MEO satellites. The mean value of the two PDOP quantities can be then associated to the edge, equally accounting for both positioning conditions determined by the established link. The use of PDOP as a weight metric can be, therefore, extended to the general case, provided that the rows in (1) are at least three, a necessary condition to obtain a positioning solution and to compute (2), because $\mathbf{H}_{i,n}^{\top}\mathbf{H}_{i,n}$ must be invertible. Our proposed PDOP-driven CPD algorithm is, therefore, suitable to any O-GNSS, equipped with at least three LCTs per MEO satellite, of which one is subjected to a scheduling algorithm.

## IV. CPD ALGORITHM

Based on the metrics, constraints, and model from the previous section, we formulate a suitable CPD method

to resolve the link assignation problem. We first list the preparation steps of the algorithm as follows.

### A. Preliminary Steps

1) *Data Collection:* The constellation under test is simulated through the AGI Systems Tool Kit software. For the current case study, the Kepler system has been simulated according to parameters in Fig. 1. Information from visibility windows (line-of-sight visibility) among satellites for potential communication and ranging is retrieved. Also, the relative positions (in azimuth and elevation [52]) during each visibility window is then exported to MATLAB in order to compute $\mathbf{H}_{i,n}$ and the PDOP values.

2) *Fixed Links:* First, FLs are analyzed to build the fixed portion of $\mathbf{H}_{i,n}$. MEO-to-MEO intra-plane links are, therefore, used to this end in the Kepler case. Thanks to the stability of such links and the symmetry of satellite distribution within orbital planes, we can consider the elements of the first two lines of $\mathbf{H}_{i,n}$ invariant both with respect to time and to the chosen MEO satellite. A partial $\mathbf{H}_{i,n}$ is, thus, computed once, from the relative position data of two arbitrarily chosen FLs with a common MEO satellite. The result will be then combined with the row determined by the SL to complete the matrix.

3) *Schedulable Links:* Relative position data for SLs (backbone-to-MEO links in Kepler) is also collected from the constellation simulator. In this phase, a FoR cone with an aperture $\alpha$ has been set as a visibility constraint for each transceiver dedicated to a possible SL. Constraint **C1** is, thus, satisfied at this step. In contrast with intraplane MEO-to-MEO links, the relative positions of satellites are, in general, continuously changing during the visibility window of SLs. This forces the third line of $\mathbf{H}_{i,n}$ to change accordingly. As a result, a different matrix (and, thus, a different PDOP value) is produced at each time instant for each MEO satellite sustaining a SL.

4) *Adjacency Matrix:* The resulting data structure is a dynamic adjacency matrix that represents $G_n$. At each time $n$, the entry $(i, j)$ of the matrix contains the PDOP value that would result after establishing a link between satellite $i$ and satellite $j$. If no visibility is possible (line-of-sight or FoR constraint), the value is set to zero. To associate zeros with the absence of edges is a common adjacency matrix convention. Nonetheless, it is worth noting that in this case the matrix entry does not represent the resulting PDOP. For the Kepler case, backbone-to-MEO links and intraplane MEO-to-MEO links can be the only nonzero values of the matrix and the indices $i$, $j$ are consistent with the ID numbers in Fig. 1.

5) *Enforcing Fixed Links:* Even though FLs are not part of the PDOP optimization process, they must be considered in the CPD algorithm. These connections are continuously established and they should be, therefore, the preferred choice when connecting two MEO satellites in the contact plan. In particular, we need to force these edges to be part of any possible minimal PDOP subgraph. According to Appendix A, to guarantee the inclusion of each nonredundant

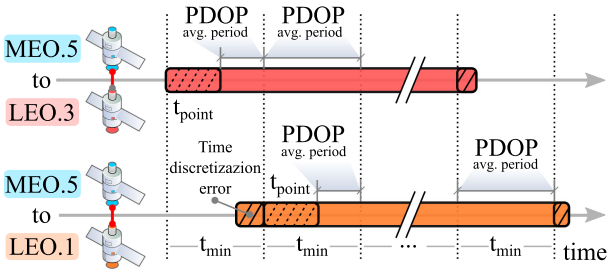


Fig. 3. Time slotting applied to visibility windows.

FL edge in our framework, it is sufficient that the weight $\varepsilon$ assigned to those edges satisfies

$$\varepsilon < \min_{i}(\mathrm{PDOP}_{i,n}) \tag{4}$$

which must hold at every time instant of the scenario (see Fig. 2). Within our model, $\varepsilon$ has been set to the smallest positive normalized floating-point number in IEEE double precision ($2^{-1022}$), satisfying this condition for the whole experiment. Notice that the fulfillment of (4) would guarantee also the inclusion of fixed LEO-to-LEO links if they are present.

### B. Time Slotting and Weight Computation

As discussed, the PDOP is the optimization metric driving the weights of the adjacency matrix. However, i) the PDOP is dynamic over a time window, and ii) each connection should exist for at least $t_{\min}$ seconds (3). To follow the time dynamics, we discretize the timeline into slots of duration $t_{\min}$ and optimize the contact plan for each of them (see Fig. 3). At the beginning of each slot, only potential connections that are continuously available for $t_{\min}$ are compared and considered for the contact plan. A link that is ultimately selected for the contact plan is, therefore, established for no less than one slot. The time slotting action satisfies **C2** and makes the problem tractable. As illustrated in Fig. 3, this comes at the price of a discretization error, causing the exclusion of the visibility window's margins from the CPD when they are shorter than $t_{\min}$. This discretization operation, however, filters out unworthy connections, that do not last for the entire slot, in favor of a potentially longer communication opportunity with another satellite in that slot, thus fostering ranging diversity.

The edge weight can, thus, be determined by averaging the instantaneous PDOP values of the corresponding slot over the upcoming communication window. However, only the PDOP experienced over the active communication portion of the visibility window is relevant for position determination. At the beginning of each $t_{\min}$ slot, a link will either ($a$) need $t_{\text{point}}$ seconds to be established for the first time, or ($b$) it can be already up and running ($t_{\text{point}}$ has already occurred in a previous slot). This means that its average PDOP should be computed over just $t_{\text{useful}}$ seconds in the first case, or over the whole $t_{\min}$ interval in the second case (see Fig. 3).

To tackle this issue, we compute two different weights for each slot, addressing ($a$) and ($b$) separately. As a result,

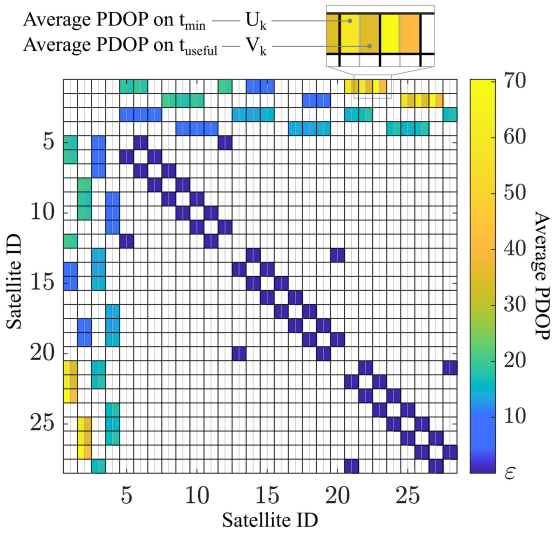


Fig. 4. Example of concurrent adjacency matrices $\mathbf{U}_k$ and $\mathbf{V}_k$. The symmetry reflects the use of bidirectional links, which must be selected concurrently. They are thus modeled with a single weight.

two concurrent adjacency matrices are obtained: $\mathbf{U}_k$ and $\mathbf{V}_k$ (see Fig. 4). Both matrices represent the available links for the $k$th upcoming $t_{\min}$ slot, but with different weights. A final adjacency matrix $\mathbf{W}_k$ is then computed at each slot $k$ by merging these two on the basis of the links that were chosen in slot $k-1$.

## C. Optimization

1) *Degree Constrained Minimum Spanning Tree:* The final adjacency matrix $\mathbf{W}_k$ represents the available connections at slot $k$ and describes a graph $G_k$ with PDOP-dependent weights. An MST could be then extracted from $G_k$ to provide a connected subgraph with minimum total edge weight (see Fig. 2). In this case, the weight $\varepsilon$ guarantees the inclusion of all intra-orbit links but one per orbital plane (cycles are also avoided by MST definition). The missing intraorbit link will be added to the tree a posteriori. This comes without loss of generality, provided that this missing—albeit existing—connection is accounted for when the limited transponders' availability is considered to fulfill constraint **C3**. In this respect, although constraints **C1** and **C2** are already satisfied in the input data to the subgraph extraction, no guarantees have been provided yet for **C3**. We need in fact to limit the maximum number of connections independently, according to the capabilities of MEO and backbone satellites, while still satisfying the MST properties. The solution to this problem is a DCMST [15]. A DMCST $M_k$ is a spanning tree of $G_k$ of minimum total weight, such that the degree of each node $i$ is at most a given value $b_i$. It is a well-known NP-hard problem [53] for which heuristics have been proposed to tackle the general formulation [15], [53]–[55] or to address the particular case of $b_i = b\,\forall i \in V$ [16]. We adapted the best performing heuristic presented in [16] to the general case and implemented it in our CPD algorithm. Through a general DCMST solution, we are able to address the transponders limitations of each satellite independently and, thus, to fulfill **C3**. The computed tree $M_k$ represents, therefore, a feasible contact plan for the $k$th slot, where the total PDOP experienced by the network is optimized on a slot basis and all the system constraints are satisfied.

Considering the Kepler case study, the three MEO orbital planes (see Fig. 1) are represented by three connected components of the graph. This means that, since no LEO-to-LEO connection exists, more than three connections per LEO satellite are impossible in an MST where FLs satisfy (4). A fourth backbone-to-MEO link would be indeed redundant. This property of the Kepler system guarantees that a plain MST extracted from $G_k$ is always compliant to constraint **C3** for what concerns LEO satellites. Moreover, the maximum degree allowed is $b = 3$ both for LEO and MEO satellites. Hence, for this system, a DCMST heuristic with $b_i = 3\,\forall i \in V$ is sufficient to comply with MEO transponders limitations as well and to satisfy **C3** for all the satellites.

2) *Secondary Optimization:* Notably, a positive-weighted DCMST includes by definition a minimal number of edges. The resulting DCMST, while minimizing the total PDOP of selected links, does not include those links that are redundant from the connectivity perspective. Indeed, although the maximum number of links assigned to each satellite is limited by the constrained degree of the tree, the satellites in the resulting network do not necessarily reach such a limit of connections. This means that there are idle LCTs left from the previous computation. Hence, since there are unexploited potential connections, a secondary optimization level may be added to the algorithm, while choosing the link to assign to the idle antennas. This further degree of freedom drove the development of four algorithm variants. All the proposed algorithms are summarized below in increasing order of complexity.

- A1. No secondary optimization added. At each slot, the resulting plan has the lowest (optimal) total PDOP, but no unessential LCTs are assigned to a connection. This conservative use of resources might be of interest if power budget needs to be considered within CPD [56]. Furthermore, it could be used as a system design input to size the number of optical transponders.
- A2. After the DCMST computation, idle LCTs are assigned to the available link that provides the lowest PDOP. Assignation stops when no other connections are possible.
- A3. This algorithm is identical to algorithm A2, but within the secondary assignment, priority is given to links that result in a single backbone satellite simultaneously connected to as many different MEO planes as possible (three for the Kepler case). This property will be referred to as B3MP priority. This criterion is addressed in [12] and we consider it for performance comparison.
- A4. After the DCMST computation, idle LCTs assignation priority is given to MEO satellites that have

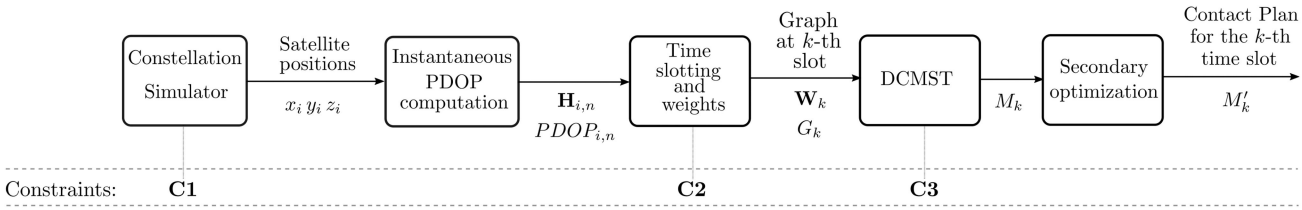


Fig. 5. Algorithms' block scheme.

the highest Revisit Time (RT), which is the time elapsed from the last SL assignation. Assignation stops when no other connections are possible.

Whatever the secondary optimization strategy applied, the algorithm is repeated at each slot. The overall contact plan is then composed by a time-sequence of graphs $M'_k$, that satisfy the objectives and constraints discussed in Section III. The complete sequence of blocks describing the CPD algorithms presented in this section is illustrated in Fig. 5 , highlighting the system constraints where fulfilled.

## V. RESULTS

In this section, we discuss the performance of the proposed CPD method applied to the Kepler case study. After the description of the performance evaluation metrics and the target scenarios, the proposed CPD algorithms are assessed and compared to existing scheduling algorithms.

### A. Performance Evaluation and Figures of Merit

A previous work on the Kepler system [12], presented two greedy algorithms for CPD, namely Scheduler I (S1) and Scheduler II (S2), that try to minimize the maximum RT of a MEO satellite with B3MP priority. Hence, although not considered as the main optimization goal, these metrics are analyzed in our simulation as well to compare them with the aforementioned schedulers. Moreover, in view of a comparative analysis with non-PDOP-driven CPD, it is worth comparing the proposed methods to two *random CPD algorithms* (R1 and R2), through which we computed a contact plan with no PDOP optimization, assigning SLs on a random basis. That is, a contact plan that merely fulfills all the constraints in Section III, regardless of the PDOP weight of each link. The link assignation can stop as soon as the whole network is connected and the constraints are satisfied (R1) or, after the fulfillment of the latter, when no more SLs can be randomly assigned (R2). The PDOP performances of such algorithms are reported to emulate those scheduling algorithms whose primary optimization goal is independent from the resulting PDOP given by the linking of satellites. Algorithms R1 and R2 are, therefore, a fair term of comparison for, respectively, an algorithm without a secondary optimization level, such as A1, and the algorithms that try to maximize the use of LCTs, such as A2, A3, and A4.

Although PDOP is the main performance metric for the proposed algorithms, other figures of merit impact the overall benefit brought by each CPD method. Indeed, the secondary optimization level is exploited to address such different aspects. Algorithm A4 for instance prioritizes the RT, which is related to the time distribution of ranging opportunities, enabled by a SL assignation. From a network point of view, a link assignation affects also the processing load of the node (the satellite), concerning both data transfer and clock distribution. It is thus relevant to analyze also the distribution of these ranging opportunities within the system. To this end, we can resort to metrics from the communications domain.

A figure of merit from such a domain is the Jain fairness index (JFI) [57], which is a measure of the equality of resource allocation in a system. It is defined as

$$\text{JFI} = \frac{\left(\sum_{i\in V} s_i\right)^2}{\sum_{i\in V} s_i^2} \tag{5}$$

where $s_i$ accounts for the resources allocated to user $i$, i.e., it is the total amount of assigned SL connections for the $i$th satellite. If all the users receive the same allocation, the index is 1 and the system is completely fair in this sense. The index approaches zero as the disparity increases.

We are interested also in the observation of the data delivery latency (DDL) of the network, defined as the number of hops necessary to connect a node to another within a specific contact plan configuration. Hence, this "distance" among satellites affects both the data and clock distribution latency and in turn, the synchronization capabilities of the system.

### B. Simulated Scenarios

We investigated four different scenarios (see Fig. 6), varying the following system parameters:

1) The FoR of LCTs dedicated to SLs, setting $\alpha = 70^\circ$ or $\alpha = 90^\circ$.
2) The size of the backbone fleet, choosing a backbone implementation with 4 or 6 LEO satellites.

Either varying parameter affects the connection opportunities. Indeed, a broader FoR or an enhanced supporting fleet increases the graph density, thus empowering the algorithms' optimization capability.

The common parameters used for the CPD simulation are summarized in Table I. A 10-days scenario is enough to simulate a sufficiently wide range of configurations while a MEO LCT cutoff angle of 29° is suitable to illuminate

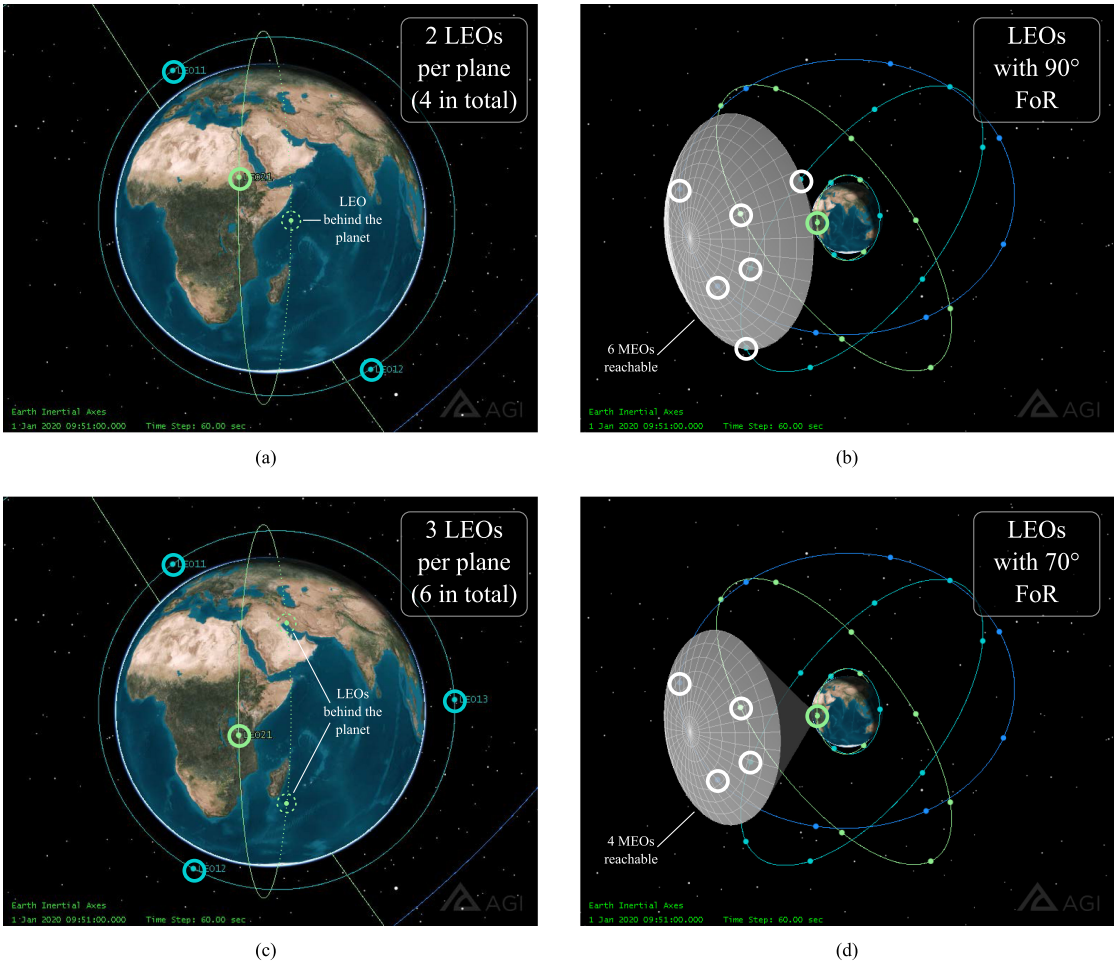


Fig. 6. Simulated scenarios varying the size of the supporting LEO fleet (4 and 6) and varying the FoR angle (90 and 70°).

TABLE I
Simulation Parameters

| Parameter | Value |
|---|---|
| Scenario duration | 10 days and 12 hours |
| Simulation time step | 30 s |
| Orbit propagator | J4 |
| $t_{min}$ | 300 s |
| $t_{point}$ | 120 s |

the whole LEO backbone [12]. A two minutes $t_{\text{point}}$ has been set according to values reported in literature [58] and experimental recommendations issued by the consultative committee for space data systems [59].

## C. Simulation Results

To give the reader an efficient and yet comprehensive means of comparison we provide the scatter plots in Fig. 7, which are a measure of the performance from a joint RT and PDOP perspective. The position of each point in a plot is determined by the average of the RT ($x$-axis) and the PDOP ($y$-axis) experienced by the constellation at a given time. The average is computed over all the MEO satellites of the network configuration $M'_k$, hence obtaining one point for each time slot $k$. This kind of plot allows a comparative analysis of the average behavior of algorithms by looking at the distribution of the clouds of points (*clusters*). The black-edged circles are the mean points of the clusters.

1) *Algorithms Comparison:* In terms of average PDOP, A1 is the best performing algorithm in all the scenarios. This comes as no surprise since this algorithm delivers the optimal PDOP configuration with the minimal use of connections. Indeed A1 provides an improved contact plan, where the optimization of the overall PDOP conditions is effective in all the network configurations $M'_k$, resulting also in a more compact cluster with respect to the other algorithms. If ranging conditions are not being considered when delivering a feasible contact plan, as with R1, the mean PDOP of the network is, on average, almost one order of magnitude worse than what A1 can provide.

For both CPD methods, however, 6 to 10 LEO LCTs are left unused on average at each time slot (see Table II). A complete exploitation of this resource would certainly reduce the average RT, which is generally higher for A1 in all the scenarios. Indeed, the latter is definitely better when a secondary optimization level is exploited since an increased LCTs utilization is pursued. Nonetheless, additional connections are likely to provide poorer PDOP conditions, because a constrained selection of the smallest PDOP links

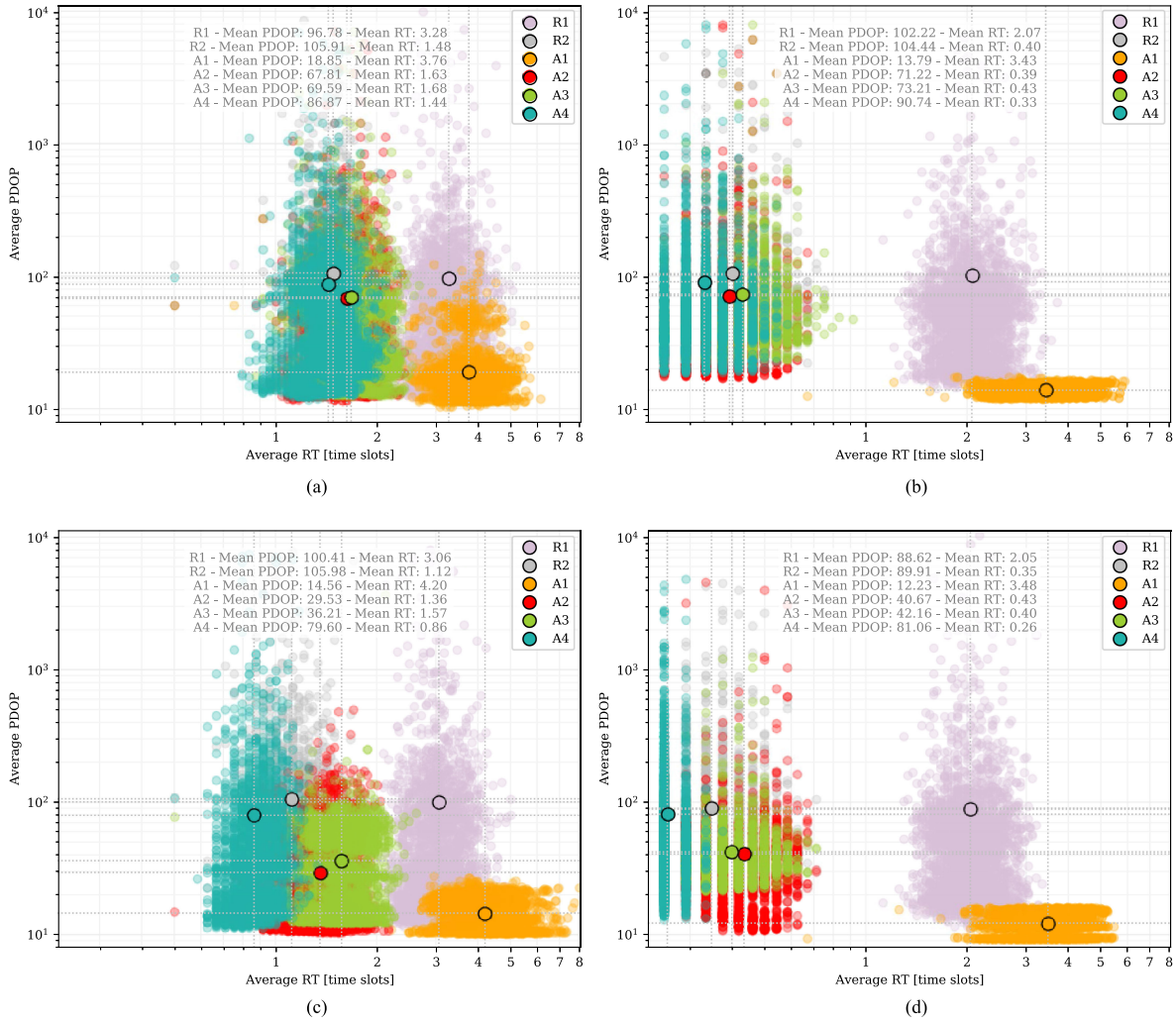


Fig. 7. PDOP and revisit time performance of the investigated algorithms. (a) 70°FoR - 4LEO. (b) 70°FoR - 6LEO. (c) 90°FoR - 4LEO. (d) 90°FoR - 6LEO.

already took place during the DCMST extraction $M_k$. Keep in mind, however, that as long as the added links bring in a profitable PDOP, an increased number of MEO satellites can improve their position estimation. In other words, an underutilization of LCT resources should be a desirable feature of the contact plan, if a method like A1 is used, providing a PDOP-optimized scheduling with a minimal use of transceivers.

With respect to A1, algorithms A2, A3, and A4 perform increasingly worse in terms of PDOP as other link assignation criteria are addressed. Within this category, A2 has the best PDOP whereas other algorithms trade an overall minimum PDOP with other objectives such as a minimized RT (A4) or a maximized number of epochs with B3MP (A3), for the benefit of the respective figures of merit (see Table II). Nonetheless, the points on the plots of Fig. 7 behave accordingly.

It is clear that, as more efforts are devoted to improving the PDOP, other figures of merit may be penalized. However, if we look at the performance of A3 and A4 through the scenarios, by means of the non-PDOP metrics reported in Table II, it can be observed that their results are comparable with those reported in [12], where positioning-related metrics (such as PDOP) are not considered as a global goal. In particular, the maximum RT experienced with A4 is always very close or even better than the maximum RT provided by the best of the two schedulers S1 and S2. On the other hand, in terms of epochs with B3MP, A3 is very close to the best of S1 and S2 in three scenarios out of four, and the same is true for A4. It is worth stressing, that in addition to these remarkable outcomes, A3 and A4 deliver a minimized average PDOP favoring profitable ranging conditions, whereas a non-PDOP-driven contact plan, like R2, does not. However, such a performance gap is slightly visible in Fig. 7, where aggregated metrics are shown. In this view, it is meaningful to analyze also the distribution of PDOP values within each network configuration $M'_k$.

The percentiles shown in Table III are computed for each network configuration of the contact plan over the entire simulation. Differently from the PDOP-driven CPD algorithms, R1 and R2 might be affected by large outliers that degrade a networkwise metric like the mean values

TABLE II
Performance Comparison of Non-PDOP Metrics

| | $\alpha = 70°$, 4 LEO | | | | | | | |
|---|---|---|---|---|---|---|---|---|
| Metrics | A1 | R1 | A2 | A3 | A4 | R2 | S1[b] | S2[b] |
| Epochs with B3MP (%)[a] | 29.89 | 17.73 | 62.24 | 79.20 | 73.81 | 51.29 | 91.95 | 92.36 |
| Maximum RT (time slots) | 46 | 37 | 11 | 11 | 8 | 12 | 9.1 | 10.5 |
| JFI | 0.9830 | 0.9989 | 0.9996 | 0.9992 | 0.9993 | 0.9955 | - | - |
| Longest DDL (hops) | 16 | 16 | 15 | 9 | 15 | 15 | - | - |
| Mean no. of idle LCTs | 6 | 6 | 0.25 | 0.34 | 0.25 | 0.17 | - | - |
| | $\alpha = 90°$, 4 LEO | | | | | | | |
| Metrics | A1 | R1 | A2 | A3 | A4 | R2 | S1 | S2 |
| Epochs with B3MP (%) | 35.38 | 28.60 | 63.06 | 100 | 90.28 | 75.73 | 100 | 100 |
| Maximum RT (time slots) | 50 | 33 | 10 | 12 | 7 | 18 | 7 | 8.2 |
| JFI | 0.9707 | 0.9989 | 0.9900 | 0.9959 | 0.9962 | 0.9993 | - | - |
| Longest DDL (hops) | 16 | 16 | 15 | 7 | 14 | 15 | - | - |
| Mean no. of idle LCTs | 6 | 6 | 0 | 0 | 0 | 0.0003 | - | - |
| | $\alpha = 70°$, 6 LEO | | | | | | | |
| Metrics | A1 | R1 | A2 | A3 | A4 | R2 | S1 | S2 |
| Epochs with B3MP (%) | 5.09 | 11.94 | 73.51 | 99.24 | 92.69 | 67.29 | 100 | 100 |
| Maximum RT (time slots) | 34 | 25 | 6 | 5 | 4 | 7 | 3.9 | 4.4 |
| JFI | 0.9467 | 0.9994 | 0.9999 | 0.9997 | 0.9994 | 0.9994 | - | - |
| Longest DDL (hops) | 16 | 16 | 10 | 8 | 10 | 12 | - | - |
| Mean no. of idle LCTs | 10 | 10 | 0.42 | 0.32 | 0.33 | 0.61 | - | - |
| | $\alpha = 90°$, 6 LEO | | | | | | | |
| Metrics | A1 | R1 | A2 | A3 | A4 | R2 | S1 | S2 |
| Epochs with B3MP (%) | 3.54 | 19.08 | 60.12 | 100 | 96.76 | 84.99 | 100 | 100 |
| Maximum RT (time slots) | 35 | 26 | 6 | 7 | 3 | 8 | 2.9 | 3.3 |
| JFI | 0.9506 | 0.9979 | 0.9807 | 0.9974 | 0.9960 | 0.9991 | - | - |
| Longest DDL (hops) | 16 | 16 | 10 | 7 | 10 | 11 | - | - |
| Mean no. of idle LCTs | 10 | 10 | 0.0073 | 0.0268 | 0.0407 | 0.0678 | - | - |

[a]Epochs with at least one backbone satellite connecting three distinct MEO orbital planes.[b]Results from [12].

TABLE III
PDOP Distribution Over the Entire Simulation

| | | $\alpha = 70°$ | | | | | | $\alpha = 90°$ | | | | | |
|---|---|---|---|---|---|---|---|---|---|---|---|---|---|
| No. of LEO satellites | Percentiles | A1 | R1 | A2 | A3 | A4 | R2 | A1 | R1 | A2 | A3 | A4 | R2 |
| 4 | 25 | 10.8 | 11.9 | 11.5 | 11.7 | 11.8 | 12.3 | 9.0 | 11.2 | 9.3 | 10.3 | 9.9 | 11.4 |
| | 50 | 12.6 | 16.0 | 14.5 | 15.4 | 16.1 | 17.1 | 10.4 | 14.4 | 11.3 | 13.6 | 13.3 | 15.3 |
| | 75 | 19.0 | 31.6 | 28.3 | 29.4 | 31.9 | 34.7 | 14.1 | 27.5 | 20.1 | 25.9 | 27.2 | 30.7 |
| | 95 | 39.0 | 283.3 | 248.0 | 255.2 | 281.3 | 304.0 | 35.5 | 288.8 | 82.8 | 167.6 | 233.9 | 322.5 |
| | 99 | 139.0 | 797.0 | 622.9 | 645.3 | 801.0 | 893.1 | 61.3 | 930.6 | 384.4 | 370.0 | 822.9 | 1003.3 |
| | 99.9 | 313.5 | 10467.5 | 4251.6 | 4382.8 | 6972.8 | 10171.9 | 97.5 | 8481.0 | 805.55 | 674.8 | 5931.4 | 9408.0 |
| 6 | 25 | 10.2 | 12.0 | 11.4 | 11.6 | 11.5 | 12.4 | 9.0 | 11.3 | 9.4 | 10.3 | 9.9 | 11.5 |
| | 50 | 11.4 | 16.8 | 14.0 | 15.9 | 15.5 | 17.5 | 9.9 | 14.7 | 11.3 | 13.5 | 12.7 | 15.4 |
| | 75 | 14.5 | 33.1 | 26.3 | 30.0 | 31.0 | 34.7 | 11.3 | 28.7 | 16.7 | 26.3 | 26.6 | 30.9 |
| | 95 | 28.2 | 295.6 | 228.0 | 252.5 | 285.4 | 304.0 | 29.2 | 287.6 | 113.7 | 207.0 | 277.6 | 311.6 |
| | 99 | 37.4 | 918.4 | 606.7 | 630.5 | 854.6 | 928.8 | 39.1 | 888.8 | 424.5 | 424.4 | 868.0 | 952.3 |
| | 99.9 | 41.7 | 8044.7 | 3887.4 | 4032.0 | 6727.2 | 7459.7 | 43.0 | 9080.2 | 1575.1 | 1253.3 | 7354.1 | 8658.2 |

shown in the plots of Fig. 7. As the percentiles increase, the difference between PDOP-driven methods and random CPD algorithms grows, confirming the latter as less robust against outliers, which in turn lead to completely unprofitable PDOP values. However, even if the highest percentiles are not considered, the PDOP-driven CPD algorithms are always advantageous and prove to be a highly effective solution in terms of orbit determination quality.

The benefits provided do not penalize other figures of merit. All the proposed algorithms present in fact a good degree of fairness, expressed by the JFI values in Table II. Ranging opportunities and the consequent orbit determination improvements are, therefore, equally distributed among the satellites. As a consequence, each of them can be reached from any other satellite in no more than 16 hops (see Table II), thus bounding the DDL and ensuring data and clock distribution in a given time. The interested reader can refer to the "Supplementary Materials" of this article, where case-by-case outcomes are inspected in detail with respect to the relevant figures of merit, focusing on the performance of each MEO satellite of the constellation.

2) *Scenarios Comparison:* A general observation can be done on the CPD algorithms associated by a maximal use of LCTs (A2, A3, A4, and R2). As it can be seen in Fig. 7, the clusters are moving closer as the linking opportunities are being limited (smaller FoR and LEO fleet). This is especially true when the FoR is limited to 70°. As more and more links are chosen, fewer potential connections are left out from the final contact plan. As the network becomes small (due to a reduced LEO fleet), and the graph of potential connections $G_k$ becomes less dense (due to limited FoR), the sets of chosen links in the various algorithms are largely

TABLE IV
Computational Time

| Algorithm | Computational Time (s) |
|---|---|
| A1 | 91.4 |
| A2 | 187.2 |
| A3 | 182.0 |
| A4 | 200.6 |

overlapped, producing similar performances. As a result, even a CPD method that disregards ranging conditions, such as R2, is not far from the other algorithms. R2 is likely to produce the worst PDOP, but, especially in the most limiting scenario [see Fig. 7(a)], its average performance is very close to the other methods. Nonetheless, a performance gap is there and it stands out when inspecting the distribution of PDOP values within the network, as mentioned, by looking at the percentiles in Table III. It is worth noting, however, that thanks to time-slotting and a heuristical approach to the DCMST problem, the proposed algorithms can be easily scaled to broader networks, where they are likely to produce a more remarkable gap.

Another effect of the scenario variation, also visible in Fig. 7, concerns the average RT. A general shift toward lower average RT values can be observed when the ranging opportunities increase, particularly in the scenarios where the backbone fleet comprises 6 LEO satellites. A similar shift is also experienced toward lower average PDOP values, but mostly when the FoR is widened. This means that the enhanced connectivity, and the larger and denser graph that goes with it, is not just favoring the algorithms' differentiation (the separation of the clusters), but also their attainable performance. The net result is in fact an enhanced capability of the various algorithms to select the best connections that satisfy their optimization criteria.

3) *Computational Time Assessment:* A possible drawback of the proposed methods w.r.t. greedy algorithms might be the increased computational complexity. The latter is however quite affordable, thanks to the heuristics employed in the process and to the time-slotting operation. The computational time of the proposed schedulers has been assessed with an Intel Core i5-6200 U CPU at 2.30 GHz, running a 5.4.0-65-generic Linux kernel. The tests were made on the scenario that challenges the routine with the largest and densest graph ($\alpha = 90^\circ$, 6 LEO), averaging the outcomes of 10 simulations. The results are reported in Table IV.

The proposed CPD methods can draw a complete scheduling plan for a 10.5 days scenario (3024 time slots), in less than 201 s, on average. The moderate computational effort makes them suitable to a timely provision of the contact plan, even for fast-changing and partially predictable geometries.

## VI. CONCLUSION

In this article, a general CPD method for GNSS constellations supported by OISLs has been presented. The technique delivers an improved contact plan which favors orbit determination conditions thanks to the use of DCMST heuristics. The approach guarantees the connection of all the satellites in the constellation while fulfilling the general constraints of optically-linked satellite networks. Four distinct algorithms have been presented and differentiated by as many optimization goals. The algorithms have been described in detail and their performances have been discussed through several figures of merit. They have been compared to existing schedulers and to CPD methods such as algorithms R1 and R2, that do not target globally optimized ranging conditions. Results have shown that our approach is advantageous in all the assessed scenarios. In particular, when minimal LCTs assignation is pursued (A1), our proposed methodology proved an average improvement of 85 % of the mean network PDOP with respect to a generic scheduler that disregards the geometrical distribution of the chosen links (R1). Furthermore, when a maximized use of available links is combined with a minimum PDOP goal (A2), the average PDOP reduction with respect to R2 is 49 %, reaching 72 % for the most favorable case (90° FoR, 4 LEO). The proposed methods favor also resource allocation fairness. The ranging opportunities are equally distributed throughout the network fostering a widespread orbit determination improvement. To this end, the time interval between consecutive ranging opportunities of each satellite has been kept under 60 min, when link assignation is maximized (A2, A3, A4). This holds even in those scenarios where the potential connections are reduced, guaranteeing a RT performance comparable with state-of-the-art schedulers, even though improved ranging conditions are potentially achieved.

Thanks to the use of heuristics and time-slotting, the proposed methods demand a limited computational effort. They could, therefore, scale to wider networks, managing the contact plan of larger and denser graphs. Further studies that would address such networks will likely show an improved performance gain of the proposed algorithms due to an empowered capability of link selection. Nonetheless, the flexibility of the proposed CPD approach allows us addressing additional case studies, characterized by alternative backbone segments (HEO, GSO) or no backbone at all. Such systems will be considered as further case studies if practical applications will arise in literature.

## APPENDIX A
## EDGE INCLUSION IN MINIMUM SPANNING TREE

FLs are not part of the optimization process. They are constantly established and moreover, they cannot be associated to a single PDOP value in our topology model (see Section III-C). However, the CPD process should be aware of existing FLs and they must be modeled through the graph framework defined for the proposed method. In the system, we are modeling, FLs are established anyway and, thus, they come at no cost. They should be, therefore, included in any contact plan as the preferred choice to connect two nodes of the network with minimum effort.

A spanning tree contains the minimum number of edges needed to connect all the nodes of an undirected graph.

Among the possible solutions, all the subgraphs whose total weight of the edges is minimum are an MST of the initial graph. We are looking for a condition on FLs that guarantees their inclusion in any MST or at least in the one we are constructing through our algorithm. To this end we, shall recall some definitions from graph theory, while others, more basic ones such as cycle, connected component, forest, and tree, are assumed as known.

DEFINITION A.1 Let a set of edges $A$ be a subset of some MST. An edge $(u, v)$ is called a *safe edge* if $A \cup \{(u, v)\}$ is also a subset of an MST.

DEFINITION A.2 An edge is a *light edge* satisfying a given property if its weight is the minimum of any edge satisfying the property. Note that in case of ties, there can be more than one light edge satisfying a given property.

The abovementioned definitions are exploited by the following corollary [60]. The theorem from which the corollary follows is omitted for the sake of brevity. The interested reader can refer to [60].

COROLLARY A.0.1 Let $G = (V, E)$ be a connected, undirected graph with a real-valued weight function $w$ defined on $E$. Let $A$ be a subset of $E$ that is included in some MST for $G$, and let $C = (V_C, E_C)$ be a connected component (tree) in the forest $G_A = (V, A)$. If $(u, v)$ is a light edge connecting $C$ to some other component in $G_A$, then $(u, v)$ is safe for $A$.

By exploiting Corollary A.0.1, we can prove the following theorem.

THEOREM A.1 Let $G = (V, E)$ be a connected, undirected graph with a real-valued weight function $w$ defined on $E$. Let $F = \{e_1, \ldots, e_N\}$ be a set of edges such that $F \subseteq E$ and $w(e_i) = \varepsilon \, \forall i : e_i \in F$. Then, if

$$\varepsilon < \min_{e_j \in E \setminus F} w(e_j) \tag{6}$$

all edges in $F$ are included in an MST of $G$ with the exception of one edge for each cycle composed solely by edges belonging to $F$.

PROOF Since $A = \emptyset$ is a subset of any MST, it follows from Corollary A.0.1 that an edge $e_i$ of minimum weight among all edges in $E$ is a safe edge for $A$. That is because a minimum weight edge is certainly a light edge connecting two connected components in the forest $G_A = (V, A)$, made by all vertices of $G$ and no edges. Therefore, $A = \{e_i\}$ is a subset of an MST. The edge with minimum weight among all the remaining edges in $E \setminus A$ is again a safe edge for $A$, as long as it connects two connected components in $G_A$. In other words, this edge should not form a cycle in $G_A$. This process can be, therefore, repeated for all the edges that satisfy (6) taken in any order, but the selected edge should not form a cycle within $G_A$, while $A$ is composed only by edges for which (6) is true. Since a cycle can be broken by removing one of its component edges, all the edges that satisfy (6) are included in an MST of $G$, with the exception of one edge per cycle made solely by the edges in $F$. ■

Notice that the edge that ultimately forms the cycle is determined by the edge inclusion order. Hence, a different inclusion order of the elements in $F$ leads to a different edge exclusion (in case of cycles) and, thus, to a different MST. Referring again to a contact plan framework, such an edge exclusion is not a problem. In fact, the excluded edge can be safely added to the contact plan, provided that such an edge has been taken into account during the optimization routine so that its eventual inclusion does not break the constraints of the system under investigation. Under these assumptions, which one of the suitable edges is excluded does not influence the final result.

## REFERENCES


[1] E. Kaplan and C. Hegarty
*Understanding GPS/GNSS: Principles and Applications*. Norwood, MA, USA: Artech House, 2017.

[2] "Galileo open service, signal in space interface control document " (OS SIS ICD V2.0)," Jan. 2021. [Online]. Available: https://www.gsc-europa.eu/electronic-library/programme-reference-documents

[3] W. Meng *et al.*
Design and experiment of onboard laser time transfer in chinese BeiDou navigation satellites
*Adv. Space Res.*, vol. 51, no. 6, pp. 951–958, 2013.

[4] Z. Yan, *et al.*
Distributed contact plan design for GNSSs
*IEEE Trans. Aerosp. Electron. Syst.*, vol. 56, no. 1, pp. 660–672, Feb. 2020.

[5] C. Günther
Kepler - satellite navigation without clocks and ground infrastructure
In *Proc. 31st Int. Tech. Meeting Satell. Division Inst. Navigation*, 2018, pp. 849–856.

[6] D. Yang, J. Yang, G. Li, Y. Zhou, and C. Tang
Globalization highlight: Orbit determination using BeiDou inter-satellite ranging measurements
*GPS Solutions*, vol. 21, no. 3, pp. 1395–1404, Jul. 2017. [Online]. Available: https://doi.org/10.1007/s10291-017-0626-5

[7] M. Menn and H. Bernstein
Ephemeris observability issues in the global positioning system (GPS) autonomous navigation (AUTONAV)
In *Proc. IEEE Position, Location Navigation Symp.*, 1994, pp. 677–680.

[8] G. Giorgi *et al.*
Advanced technologies for satellite navigation and geodesy
*Adv. Space Res.*, vol. 64, no. 6, pp. 1256–1273, 2019.

[9] K. U. Schreiber, *et al.*
Ground-based demonstration of the european laser timing (ELT) experiment
*IEEE Trans. Ultrason., Ferroelectr., Freq. Control*, vol. 57, no. 3, pp. 728–737, Mar. 2010.

[10] P. Henkel
Precise point positioning with kepler
In *Proc. IEEE 90th Veh. Technol. Conf.*, 2019, pp. 1–5.

[11] S. G. Francisco
GPS operational control segment
*Global Positioning System: Theory Appl.*, vol. 1, pp. 435–466, 1996.

[12] G. Giorgi, B. Kroese, and G. Michalak
Future GNSS constellations with optical inter-satellite links. preliminary space segment analyses
In *Proc. IEEE Aerosp. Conf.*, 2019, pp. 1–13.

[13] M. Gregory, F. F. Heine, H. Kämpfner, R. Lange, M. Lutzer, and R. Meyer
Commercial optical inter-satellite communication at high data rates
*Opt. Eng.*, vol. 51, no. 3, 2012, Art. no. 031202.

[14] J. A. Fraire and J. M. Finochietto
Design challenges in contact plans for disruption-tolerant satellite networks
*IEEE Commun. Mag.*, vol. 53, no. 5, pp. 163–169, May 2015.

[15] S. Narula and C. Ho
Degree-constrained minimum spanning tree
*Comput. Operations Res.*, vol. 7, no. 4, pp. 239–249, 1980.

[16] B. Boldon, N. Deo, and N. Kumar
Minimum-weight degree-constrained spanning tree problem: Heuristics and implementation on an SIMD parallel machine
*Parallel Comput.*, vol. 22, no. 3, pp. 369–382, 1996.

[17] G. X. Gao and P. Enge
How many GNSS satellites are too many?
*IEEE Trans. Aerosp. Electron. Syst.*, vol. 48, no. 4, pp. 2865–2874, Oct. 2012.

[18] Y. Yang, W. Gao, S. Guo, Y. Mao, and Y. Yang
Introduction to BeiDou-3 navigation satellite system
*NAVIGATION, J. Inst. Navigation*, vol. 66, no. 1, pp. 7–18, 2019. [Online]. Available: https://onlinelibrary.wiley.com/doi/abs/10.1002/navi.291

[19] S. Liu, J. Yang, X. Guo, and L. Sun
Inter-satellite link assignment for the laser/radio hybrid network in navigation satellite systems
*GPS Solutions*, vol. 24, no. 2, Feb. 2020, Art. no. 49. [Online]. Available: https://doi.org/10.1007/s10291-020-0961-9

[20] O. Luba, L. Boyd, A. Gower, and J. Crum
GPS III system operations concepts
*IEEE Aerosp. Electron. Syst. Mag.*, vol. 20, no. 1, pp. 10–18, Jan. 2005.

[21] M. Sánchez, J. Pulido, F. Amarillo, and J. Gerner
The ESA GNSS project. inter-satellite ranging and communication links in the frame of the GNSS infrastructure evolutions
In *Proc. 21st Int. Tech. Meeting Satell. Division Inst. Navigation*, 2008, pp. 2538–2546.

[22] F. A. Fernández
Inter-satellite ranging and inter-satellite communication links for enhancing GNSS satellite broadcast navigation data
*Adv. Space Res.*, vol. 47, no. 5, pp. 786–801, 2011.

[23] J. Huang, Y. Su, W. Liu, and F. Wang
Adaptive modulation and coding techniques for global navigation satellite system inter-satellite communication based on the channel condition
*IET Commun.*, vol. 10, no. 16, pp. 2091–2095, 2016.

[24] S. Han, Q. Gui, and J. Li
Establishment criteria, routing algorithms and probability of use of inter-satellite links in mixed navigation constellations
*Adv. Space Res.*, vol. 51, no. 11, pp. 2084–2092, 2013.

[25] F. Dong, J. Lv, Y. Yu, Q. Wang, and C. Wang
Inter-satellite traffic data modeling for GNSS
In *Proc. China Satellite Navigation Conf.*, J. Sun, J. Liu, Y. Yang, and S. Fan, Eds., Berlin, Heidelberg, Springer, 2012, pp. 69–78.

[26] D. Giggenbach, J. Horwath, and M. Knapek
"Optical data downlinks from Earth observation platforms ," in *Proc. SPIE 7199, Free-Space Laser Commun. Technol. XXI*, 2009, pp. 17–30, doi: 10.1117/12.811152.

[27] A. Biswas, B. Oaida, K. S. Andrews, J. M. Kovalik, M. Abrahamson, and M. W. Wright
Optical payload for lasercomm science (OPALS) link validation during operations from the ISS
In *Free-Space Laser Communication and Atmospheric Propagation XXVII*, H. Hemmati and D. M. Boroson, Eds., vol. 9354. Bellingham, WA, USA: Int. Soc. Opt. Photon., 2015, pp. 123–132. [Online]. Available: https://doi.org/10.1117/12.2084964

[28] C. Fuchs *et al.*
Sota optical downlinks to DLR's optical ground stations
In *Proc. Int. Conf. Space Optics*, B. Cugny, N. Karafolas, and Z. Sodnik,
Eds., *Int. Soc. Opt. Photon*. SPIE, 2017, pp. 1228–1236. [Online]. Available: https://doi.org/10.1117/12.2296107

[29] D. Tröndle, *et al.*
Alphasat-Sentinel-1 A optical inter-satellite links: Run-up for the European data relay satellite system
In *Free-Space Laser Communication and Atmospheric Propagation XXVIII*, H. Hemmati and D. M. Boroson, Eds., vol. 9739. Bellingham, WA, USA: *SPIE*, 2016, pp. 1–6. [Online]. Available:https://doi.org/10.1117/12.2212744

[30] D. M. Boroson *et al.*
Overview and results of the Lunar Laser Communication Demonstration
in Free-Space Laser Communication and Atmospheric Propagation XXVI, H. Hemmati and D. M. Boroson, Eds., vol. 8971. Bellingham, WA, USA: Int. Soc. Opt. Photon., 2014, pp. 213–223. [Online]. Available:https://doi.org/10.1117/12.2045508

[31] B. Rödiger, *et al.*
High data-rate optical communication payload for cubesats
In *Laser Commun. Propag. Through Atmosphere Oceans IX*, vol. 11506. Bellingham, WA, USA: Int. Soc. Opt. Photon., 2020, Art. no. 1150604.

[32] P. Exertier, *et al.*
Time transfer by laser link: Data analysis and validation to the ps level
*Adv. Space Res.*, vol. 54, no. 11, pp. 2371–2385, 2014.

[33] L. Shi, W. Xiang, and X. Tang
A link assignment algorithm for GNSS with crosslink ranging
In *Proc. Int. Conf. Localization GNSS*, 2011, pp. 13–18.

[34] S. Han, Q. Gui, G. Li, and Y. Du
Minimum of PDOP and its applications in inter-satellite links (ISL) establishment of walker-$\delta$ constellation
*Adv. Space Res.*, vol. 54, no. 4, pp. 726–733, 2014.

[35] L. Jing, Z. Tianjiao, and Y. Gangqiang
Satellite-ground TT&C united scheduling methods of GNSS constellation based on nodes constraint
In *Proc. China Satellite Navigation Conf. Proc.: Volume I*, Berlin, Heidelberg, Springer, 2015, pp. 55–66.

[36] H. Yan, Q. Zhang, Y. Sun, and J. Guo
Contact plan design for navigation satellite network based on simulated annealing
In *Proc. IEEE Int. Conf. Commun. Softw. Netw.*, 2015, pp. 12–16.

[37] J. Huang, W. Liu, Y. Su, and F. Wang
Cascade optimization design of inter-satellite link enhanced with adaptability in future GNSS satellite networks
*GPS Solutions*, vol. 22, no. 2, Feb. 2018, Art. no. 44.

[38] C. Xiaogeng and C. Yuning
Time division inter-satellite link topology generation problem: Modeling and solution
*Int, J. Satell. Commun. Netw.*, vol. 36, no. 2, pp. 194–206, 2017.

[39] J. Huang, Y. Su, W. Liu, and F. Wang
Optimization design of inter-satellite link (ISL) assignment parameters in GNSS based on genetic algorithm
*Adv. Space Res.*, vol. 60, no. 12, pp. 2574–2580, 2017.

[40] D. Yang, J. Yang, and P. Xu
Timeslot scheduling of inter-satellite links based on a system of a narrow beam with time division
*GPS Solutions*, vol. 21, no. 3, pp. 999–1011, Jul. 2017.

[41] L. Sun, Y. Wang, W. Huang, J. Yang, Y. Zhou, and D. Yang
Inter-satellite communication and ranging link assignment for navigation satellite systems
*GPS Solutions*, vol. 22, no. 2, Jan. 2018, Art. no. 38.

[42] O. Montenbruck, *et al.*
GNSS satellite geometry and attitude models
*Adv. Space Res.*, vol. 56, no. 6, pp. 1015–1029, 2015.

[43] C. Tang *et al.*
Initial results of centralized autonomous orbit determination of the new-generation BDS satellites with inter-satellite link measurements
*J. Geodesy*, vol. 92, no. 10, pp. 1155–1169, 2018. [Online]. Available: https://doi.org/10.1007/s00190-018-1113-7

[44] X. Xie *et al.*
Precise orbit determination for BDS-3 satellites using satellite-ground and inter-satellite link observations
*GPS Solutions*, vol. 23, no. 2, 2019, Art. no. 40. [Online]. Available: https://doi.org/10.1007/s10291-019-0823-5

[45] H. Xu, J. Wang, and X. Zhan
Autonomous broadcast ephemeris improvement for GNSS using inter-satellite ranging measurements
*Adv. Space Res.*, vol. 49, no. 6, pp. 1034–1044, 2012. [Online]. Available: https://www.sciencedirect.com/science/article/pii/S0273117712000245

[46] X. Gong, D. Huang, S. Cai, L. Zhou, L. Yuan, and W. Feng
Parameter decomposition filter of BDS-3 combined orbit determination using inter-satellite link observations
*Adv. Space Res.*, vol. 64, no. 1, pp. 88–103, 2019. [Online]. Available: https://www.sciencedirect.com/science/article/pii/S027311771930198X

[47] J. Yan, L. Xing, P. Wang, L. Sun, and Y. Chen
A scheduling strategy to inter-satellite links assignment in GNSS
*Adv. Space Res.*, vol. 67, no. 1, pp. 198–208, 2021. [Online]. Available: https://www.sciencedirect.com/science/article/pii/S0273117720306694

[48] R. B. Langley
Dilution of precision
*GPS World*, vol. 10, no. 5, pp. 52–59, 1999.

[49] F. Harary and G. Gupta
Dynamic graph models
*Math. Comput. Model.*, vol. 25, no. 7, pp. 79–87, 1997.

[50] J. Holm, K. de Lichtenberg, and M. Thorup
Poly-logarithmic deterministic fully-dynamic algorithms for connectivity, minimum spanning tree, 2-edge, and biconnectivity
*J. ACM*, vol. 48, no. 4, pp. 723–760, Jul. 2001. [Online]. Available: https://doi.org/10.1145/502090.502095

[51] R. L. Graham and P. Hell
On the history of the minimum spanning tree problem
*Ann. Hist. Comput.*, vol. 7, no. 1, pp. 43–57, 1985.

[52] P. Banerjee and A. Bose
Evaluation of GPS PDOP from elevation and azimuth of satellites
*Indian J. Radio Space Phys.*, vol. 25, pp. 110–113, 1996.

[53] A. Ning, L. Ma, and X. Xiong
A new algorithm for degree-constrained minimum spanning tree based on the reduction technique
*Prog. Natural Sci.*, vol. 18, no. 4, pp. 495–499, 2008.

[54] X. Sun, C. Chang, H. Su, and C. Rong
Novel degree constrained minimum spanning tree algorithm based on an improved multicolony ant algorithm
*Math. Problems Eng.*, vol. 2015, 2015, Art. no. 601782.

[55] M. Krishnamoorthy, A. T. Ernst, and Y. M. Sharaiha
Comparison of algorithms for the degree constrained minimum spanning tree
*J. Heuristics*, vol. 7, no. 6, pp. 587–611, 2001.

[56] J. A. Fraire, G. Nies, C. Gerstacker, H. Hermanns, K. Bay, and M. Bisgaard
Battery-aware contact plan design for LEO satellite constellations: The ulloriaq case study
*IEEE Trans. Green Commun. Netw.*, vol. 4, no. 1, pp. 236–245, Mar. 2020.

[57] R. Jain, D. Chiu, and W. Hawe
A quantitative measure of fairness and discrimination for resource allocation in shared computer systems
DEC Res. Rep. TR-301, Sep. 1984.

[58] M. Guelman, A. Kogan, A. Kazarian, A. Livne, M. Orenstein, and H. Michalik
Acquisition and pointing control for inter-satellite laser communications
*IEEE Trans. Aerosp. Electron. Syst.*, vol. 40, no. 4, pp. 1239–1248, Oct. 2004.

[59] *Optical High Data Rate (HDR) Communication - 1064 nm*, Consultative Committee for Space Data Systems (CCSDS), 141.11-O-1, Dec. 2018. [Online]. Available: https://public.ccsds.org/Pubs/141x11o1e2.pdf

[60] T. H. Cormen, C. E. Leiserson, R. L. Rivest, and C. Stein
*Introduction to Algorithms*. Cambridge, MA, USA: MIT Press 2009, *ch. Minimum Spanning Trees*, pp. 624–629.

**Andrea Nardin** (Graduate Student Member, IEEE) received the M.Sc. degree in telecommunications engineering (*with a thesis on cooperative GNSS ranging integration in positioning algorithms*) in 2018 from Politecnico di Torino, Turin, Italy, where he is currently working toward the Ph.D. degree in electrical, electronics and communications engineering *(with the Navigation Signal Analysis and Simulation (NavSAS) group)* with the Department of Electronics and Telecommunications.

He is currently a Visiting Doctoral Researcher with Northeastern University, Boston, MA, USA. His research interests include innovative signal processing architectures and signal design for GNSS and LEO PNT.

**Juan A. Fraire** (Senior Member, IEEE) received the Ph.D. in applied sciences from Córdoba National University (UNC), Argentina in 2015. He is Researcher with Univ Lyon, Inria, INSA Lyon, CITI, Villeurbanne, France, Assistant Researcher with the National Research Council of Argentina and an Associate Professor with Universidad Nacional de Córdoba (UNC, FAMAF) and Saarland University, Germany. He is the founder and chair of the annual Space-Terrestrial Internetworking Workshop, has coauthored more than 45 papers published in international journals and leading conferences, and has imprinted a novel networking vision in his *Delay-Tolerant Satellite Network* (IEEE, New York, NY, USA). He participates in joint projects with NASA's Jet Propulsion Laboratory and the Argentinian Space Agency and collaborates with world-renowned space companies. His research interests include spaceborne networking and distributed applications enabled by state-of-the-art informatics techniques.

**Fabio Dovis** (Member, IEEE) was born in Bruino, Italy, in 1970. He received the M.Sc. degree in electronics engineering and Ph.D. degree in electronics and communications engineering from Politecnico di Torino, Turin, Italy, in 1996 and 2000, respectively.

He was with the Department of Electronics and Telecommunications, Politecnico di Torino, as an Assistant Professor in 2004 and since 2014, he has been Associate Professor with the Department of Electronics and Telecommunications, Politecnico di Torino, where he coordinates the Navigation Signal Analysis and Simulation research group. He has a relevant experience in European projects in satellite navigation as well as cooperation with industries and research institutions. His research interests include the design of GPS and Galileo receivers and advanced signal processing for interference and multipath detection and mitigation, as well as ionospheric monitoring.

Mr. Dovis is a member of the IEEE AEROSPACE AND ELECTRONICS SYSTEMS SOCIETY NAVIGATION SYSTEMS PANEL.